Wide-Angle Radiation Due to Rough Phase Fronts

By C. DRAGONE and D. C. HOGG

(Manuscript received March 8, 1963)

Nonuniformities in the phase fronts of electromagnetic and acoustical waves give rise to radiation in directions other than that desired. The magnitude of this effect is discussed here with special reference to quasi-random roughness. It is found that the level of wide-angle radiation is a strong function of the phase deviations and that reflecting surfaces, for example, should be held to tolerances of about $\pm 0.01\lambda$ to prevent the level of the wide-angle radiation from exceeding twice that due to a perfectly smooth reflector.

I. INTRODUCTION

A rough or nonuniform phase front, be it acoustical, radio, or optical, usually degrades the desired performance of components which transmit, reflect, or receive the wave. The effect is well known in the field of microwave antennas, where lenses are required to have sufficient homogeneity of dielectric constant and reflectors sufficient smoothness of surface to produce uniform phase fronts. Likewise, the quality of optical components is specified, among other things, by ability to reproduce or modify wavefronts in a prescribed manner without undue distortion.

If roughness is introduced into a wavefront by a component, some of the power is no longer radiated in the desired specular direction; it propagates at angles well removed from that direction. This effect can be described by a system of modes in the radiating aperture, each of which radiates in a specified direction.*

In practice, it is difficult to describe the roughness properly. Consider, for example, the reflector of a microwave antenna. If large, seldom is it constructed from a single sheet of metal. More often, sheets are cut and shaped to form modules of given dimension, these then being assembled with the desired precision to construct the antenna. One might expect, therefore, that the power spectrum of the wavefront would have a com-

* Often called the angular power spectrum.

ponent at a spatial wavelength related to the module dimension. Inevitably, there is also a somewhat random component. Only in special cases can one estimate the predominant spatial wavelengths in the random case. For example, if an optical component is ground with particles of given average diameter, then the roughness may be expected to have a corresponding spatial period. In the discussion that follows, we will be concerned mainly with the problem in its relationship to microwave antennas.

Degradation of the radiation patterns of microwave antennas in the vicinity of the main beam due to various phase errors has been studied quite thoroughly.[1,2] From these studies it is often concluded that $\lambda/16$ is a suitable tolerance for reflector surfaces as far as the main beam and immediate side lobes are concerned. The purpose here is to investigate the effect of phase error on that portion of the radiation pattern well removed from the main beam, i.e., the far or wide-angle lobes. For example, we question whether $\pm\lambda/16$ is a suitable tolerance for receiving antennas at earth stations of space communications systems, since in this application the far side lobes control significantly the amount of noise that enters the antenna due to radiation from the earth. At the same time, these lobes influence the amount of man-made interference that such a receiving antenna will withstand. Likewise, one requires that the radiation pattern of transmitting antennas be as clean as possible, thus permitting only the least possible radiation to be propagated in directions other than that of the main beam.

A description of the radiating modes is given first (in one dimension). The circular aperture is then discussed as a specific example. Single sinusoidal phase errors and quasi-random errors constructed from multiple sinusoids are treated. From these calculations, it is concluded that $\pm 0.01\lambda$ is a desirable tolerance for reflecting surfaces of good quality. Finally, the calculation is compared with some experimental data.

II. THE ONE-DIMENSIONAL CASE

Consider a rectangular aperture with sides of length a, b. The center of the aperture is taken as the origin of a Cartesian system of coordinates, and the x, y axes lie in the plane of the aperture. For descriptive purposes, the electric field existing within the aperture is assumed of constant amplitude and directed in the y direction, $E_{ay} = E_0 e^{j\psi(x)}$, where $\psi(x)$ is the phase error. The exponential $e^{j\psi(x)}$ can be expanded in its Fourier series

$$e^{j\psi(x)} = \sum_{n=-\infty}^{\infty} A_n \exp \frac{jn2\pi x}{a} \tag{1}$$

n being a positive integer. One has

$$e^{j\psi(x)}e^{-j\psi(x)} = 1. \tag{2}$$

By means of (1), one can express the field over the aperture as a sum of the partial fields E_{an}

$$E_{an} = E_0\left(A_n \exp\frac{jn2\pi x}{a} + A_{-n} \exp\frac{-jn2\pi x}{a}\right) \tag{3}$$

n being the number of sinusoidal phase deviations across the aperture. These elementary modes satisfy the orthogonality relation

$$\int_{-a/2}^{a/2} E_{an}E_{am}\,dx = 0 \qquad \text{if } n \neq m.$$

Then the power P radiated by the aperture is given by the sum of the powers P_n radiated by each mode.

$$P = \sum_0^\infty P_n .$$

The radiation field associated with the nth mode can be derived from the magnetic Hertzian potential directed along the z axis[3]

$$(\Pi_z)_n = \frac{-a}{n2\pi\omega\mu}\, e^{-jh_nz}\left[A_n \exp\frac{jn2\pi x}{a} - A_{-n} \exp\frac{-jn2\pi x}{a}\right] \tag{4}$$

where $h_n = k_0\sqrt{1 - (n/n_0)^2}$, $k_0 = 2\pi/\lambda$ and $n_0 = a/\lambda$. The component of the magnetic field associated with E_{an} in the plane of the aperture is given by $(H_x)_n(Z_z)_n = (E_y)_n$, $(Z_z)_n$ being the wave impedance of the nth mode measured in the z direction and $(E_y)_n = j\omega\mu\,\partial(\Pi_z)_n/\partial x$. That is

$$Z_n = (E_y/H_x)_n = (h_n/k_0)^{-1}Z_0 = Z_0\left(\sqrt{1 - (n/n_0)^2}\right)^{-1}. \tag{5}$$

Z_0 is the intrinsic impedance for a plane wave. After integrating the z component of the Poynting vector over the aperture, one has

$$P_n = b\int_{-a/2}^{a/2} |\, E_{an}\,|^2\, 1/Z_n\,dx. \tag{6}$$

When $n > n_0$, the wave impedance is imaginary and no real power is radiated in the nth mode, in which case P_n corresponds to production of a storage field. When $n < n_0$, P_n is real, and the nth mode radiates principally in the directions

$$\sin\theta = \pm n/n_0 \tag{7}$$

where θ is measured with respect to the z axis in the x-z plane. This fact

can be readily seen from (3) by noting that the nth mode can be thought to be generated in the aperture plane by the superposition of two plane waves traveling in the two directions $\pm\theta$. The amplitudes of these two plane waves are given by E_0A_n, E_0A_{-n}. If one substitutes $n_0 = a/\lambda$ in (7), the grating formula $\sin\theta = \pm n\lambda/a$ results.

In the geometrical optics approximation, these two components would radiate all the power in the two mentioned directions. Indeed, according to the diffraction phenomena, the radiation pattern of E_{an} has two main lobes of amplitudes A_nE_0, $A_{-n}E_0$, directed in the above-mentioned directions. Further, one finds that the patterns of all other components have zeroes there.

The radiation pattern generated by E_{a0} is then the only one to contribute to the power radiated per unit solid angle along the axis of the aperture. This power is proportional to $|A_0|^2$. Remembering that $A_0 = 1$ when $\psi(x) = 0$, one finds that $1 - |A_0|^2$ gives the decrease in gain of the aperture caused by the phase error $\psi(x)$. From (6), the power radiated by the higher-order modes ($n > 0$) is given by

$$\begin{aligned} P_n &= \frac{abE_0^2}{Z_0}(|A_n|^2 + |A_{-n}|^2)\sqrt{1 - (n/n_0)^2} \\ &= P_a(|A_n|^2 + |A_{-n}|^2)\sqrt{1 - (n/n_0)^2} \end{aligned} \tag{8}$$

where $P_a = abE_0^2/Z_0$ is the power radiated by the aperture when $\psi(x) = 0$.*

III. THE CIRCULAR APERTURE

Consider the circular aperture of Fig. 1. Let the field distribution be given by

$$[1 - \alpha(2\rho/D)^2]e^{j\psi} \tag{9}$$

where ψ is the phase error and a square-law taper of amplitude α has been considered. The radiation pattern of the aperture of diameter D is then given by[1]

$$g(u,\varphi) = D^2/4 \int_0^{2\pi}\int_0^1 (1 - r^2\alpha)re^{j\psi}\, e^{jur\cos(\varphi-\varphi')}\, dr\, d\varphi' \tag{10}$$

* If $n \ll n_0$, then $Z_n \approx Z_0$ and $P_n \approx P_a(|A_n|^2 + |A_{-n}|^2)$. The total power radiated by the higher modes represents an increase in the power radiated in the side lobe region of the radiation pattern. Let P_s be this power; then

$$P_s \approx P_a \sum_{n\neq 0} |A_n|^2.$$

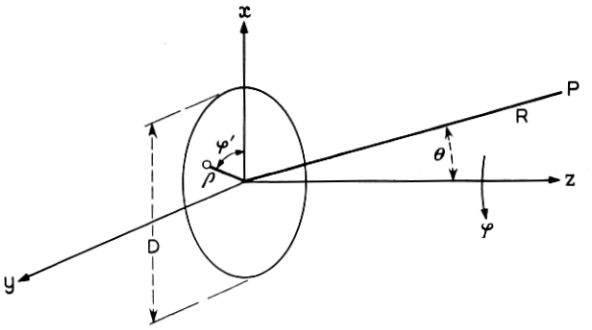

Fig. 1 — Aperture and coordinates.

where $u = (\pi D/\lambda) \sin \theta$ and $r = 2\rho/D$ is the normalized radial coordinate, θ being the angle between the antenna axis and the field point.*

Let us now consider a radial phase error $\psi = \psi(\rho)$. In this case the pattern is symmetrical about the aperture axis, and after performing the integration over φ', (10) becomes

$$g(u) = \pi D^2/2 \int_0^1 (1 - \alpha r^2) \cdot r \cdot e^{j\psi} \cdot J_0(ur)\, dr. \tag{11}$$

When $\psi = 0$, integration of (11) is readily performed and the result after normalization is

$$g_1(u) = 2(1 - \alpha) J_1(u)/u + 4\alpha J_2(u)/u^2 \tag{12}$$

where $J_p(u)$ is the Bessel function.

Different types of phase error ψ will now be considered, and the resulting radiation patterns will be compared in the far side lobe region with the ideal case given by $\psi = 0$. In all cases, since we are considering specifically paraboloidal antennas, the amplitude of the aperture field will be assumed to taper in square-law fashion to -10 db at the edge. After substituting the appropriate value of 0.684 for α in (12), one obtains the ideal pattern with no phase error shown in Fig. 2.

3.1 *Effect of Single Sinusoidal Errors*

Rather than expand the function $e^{j\psi}$ in a series as described in Section II, we choose here to expand the phase itself in a series for purpose of

* There are criticisms of the Huygens-Kirchhoff diffraction theory, especially when calculations are made at angles well removed from the axis; although some of the criticisms are known to be valid, we ignore them for these calculations. The $(1 + \cos \theta)$ factor is neglected; it can readily be multiplied in for any given antenna.

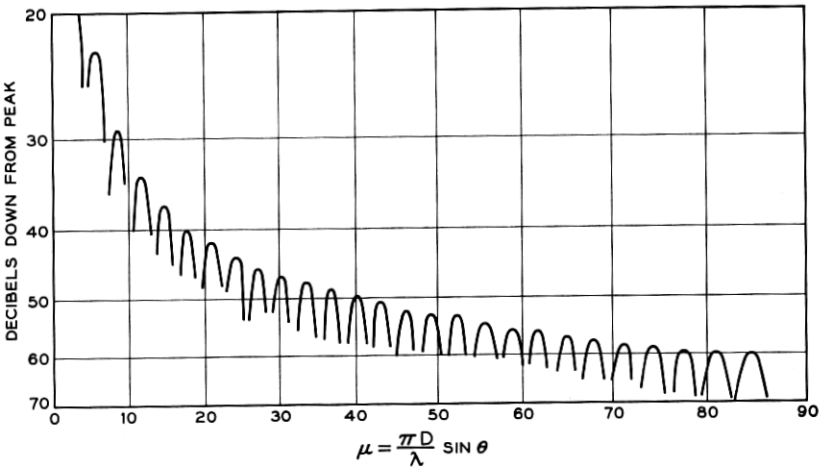

Fig. 2 — Radiation pattern for zero phase error; illumination 10-db taper.

computation. Thus by means of (11), $g(u)$ is calculated for single sinusoidal phase errors of various periods; that is, for

$$\psi = \Phi_m \cos (2\pi m r) \tag{13}$$

m being the number of periods along the aperture radius. The cases $m = 6$ and 12 for $\Phi = 2\pi/16$ have been computed and the results are plotted* in Fig. 3.

The curves of Figs. 3(a) and 3(b) show that a sinusoidal phase error causes a large disturbance only in a relatively small angular region of the radiation pattern and that these regions are located at angles which increase with the number of fluctuations in the phase distribution. The level of the disturbance depends upon the amplitude of Φ and is sensibly independent of m for the cases considered. Clearly, these disturbances are simply related to the various radiation modes discussed in Section II. For example, in Fig. 3(b) where $m = 12$, a disturbance occurs at $u = 75$; this same value is calculated by substituting $n = 2m = 24$ in (7) for $\sin \theta$, thereby evaluating the appropriate u. Thus Fig. 3(b) shows the effect of mode Π_{z24} described by (4).

Data other than those given in Fig. 3 show that there is little overlapping of adjacent disturbances, for example, between patterns for $m = 6$ and $m = 7$. In Fig. 3(a), note that a small "second harmonic" disturb-

* The patterns are plotted in decibels below the peak value. Since the peak value (the gain) is reduced only slightly due to the small phase errors considered here, the correction is neglected.

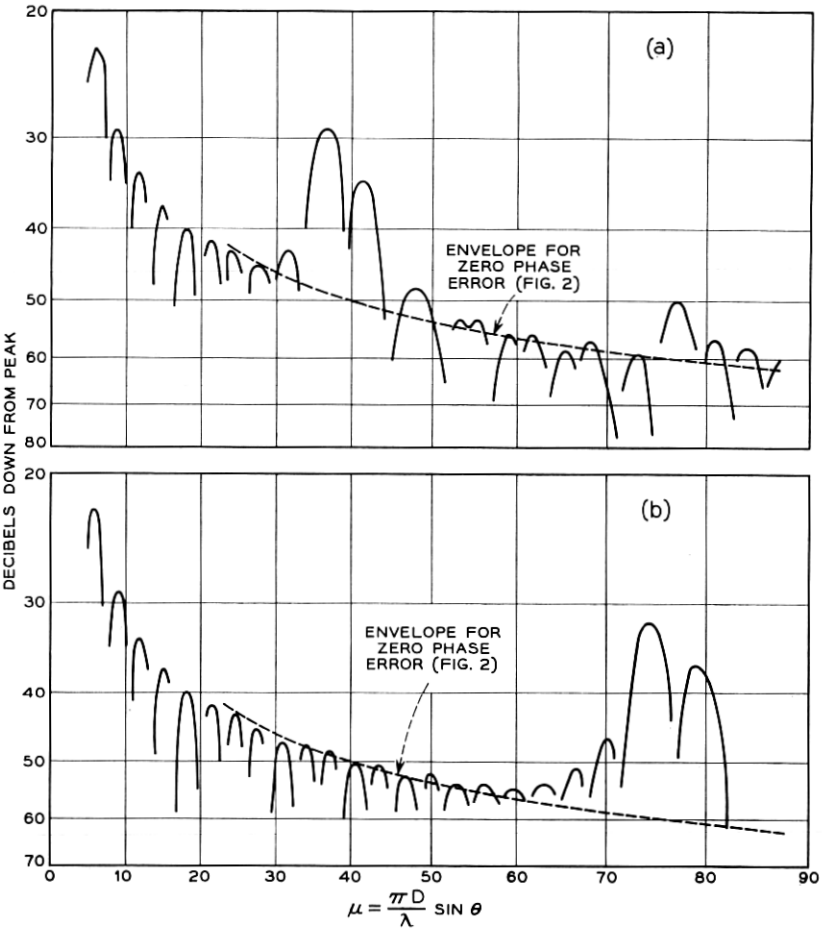

Fig. 3 — Radiation patterns — single sinusoidal phase error. (a) $m = 6$; maximum phase error, $\lambda/8$ peak-to-peak; illumination 10-db taper. (b) $m = 12$; maximum phase error, $\lambda/8$ peak-to-peak; illumination 10-db taper.

ance is evident at $u \approx 80$; this is the position of a second-order fringe if the aperture is interpreted as a weak grating.

3.2 *The Effect of a Typical Phase Error*

Let us now construct from many sinusoidal components a phase error given by the Fourier series

$$\psi = \Phi\left(\sum_{m=1}^{M} \sin\left(2\pi m[r - (m-1)/2M - \tfrac{1}{4}]\right)\right) \qquad (14)$$

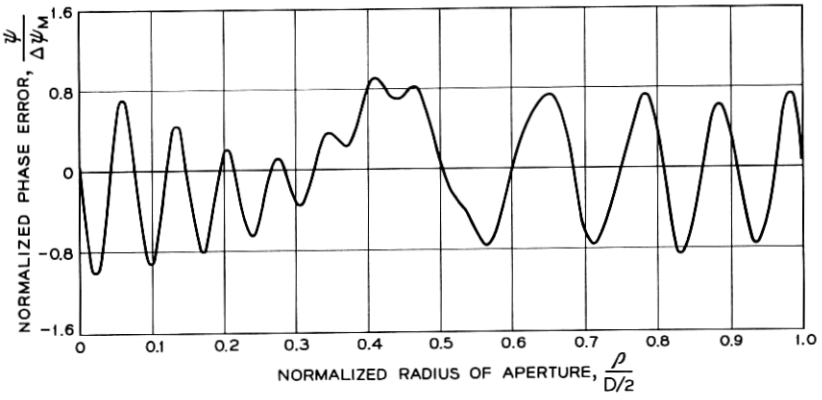

Fig. 4 — Typical phase error derived from 15 sinusoidal components of equal amplitude.

in which the M coefficients are of constant amplitude $\Phi_m = \Phi$. If the spectrum of roughness were known, the Φ_m would be written as a function of r at this point. By means of the term $(m - 1)/2M$, the phase of each component is (somewhat arbitrarily) shifted so that ψ does not have excessive irregularities and has a reasonable peak-to-peak value, $\Delta\psi_M$, between the maximum and minimum value of ψ. The phase distribution resulting from (14) is plotted in Fig. 4 for the case $M = 15$; the resulting peak-to-peak phase for this example turns out to be $\Delta\psi_M = 9.95\varphi$. Of course, one can see certain regularities in the function; but as mentioned previously, in practice these would be related to the design of any given reflector.

Radiation patterns have been computed using the phase function of Fig. 4; these are plotted in Figs. 5, 6, and 7 for peak-to-peak phase ($\Delta\psi_M$) of 0.31λ, 0.155λ, and 0.1λ, respectively.

In Fig. 8, the envelopes of the patterns shown in Figs. 5, 6, and 7 are compared with that of the ideal pattern, $\Delta\psi_M = 0$. Beyond $u \approx 30$, Fig. 8 shows, for example, that wide-angle radiation is 10 to 15 db above the ideal case if the peak-to-peak phase error is 0.155λ (roughly equivalent to a reflector with tolerance $\pm\lambda/25$). Also shown in Fig. 8 is the envelope for $\Delta\psi_M = 0.048\lambda$, in which case the far side lobes are about 3 db above the ideal case.

Since data have been computed for five values of phase error (including zero), we may plot degradation in side lobe level relative to the ideal case versus peak-to-peak phase error for various angles from the desired direction of propagation. That plot is shown in Fig. 9 for angles corresponding to $u = 50$.

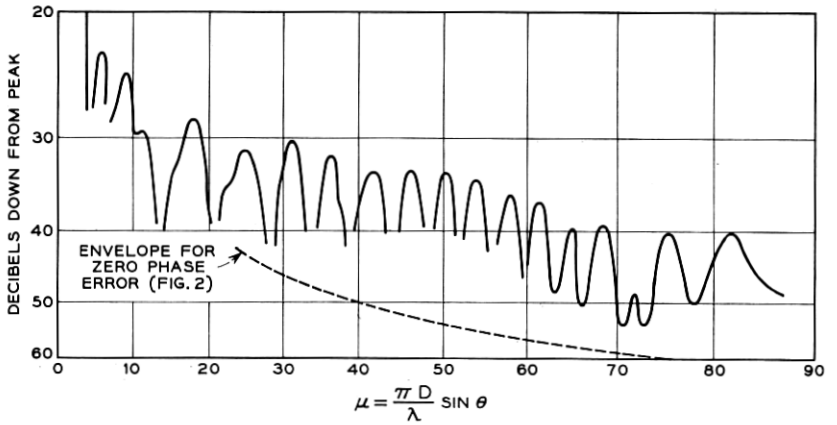

Fig. 5 — Radiation pattern: typical phase error — maximum phase error 0.31λ peak-to-peak; illumination 10-db taper.

Let us now define a good radiation pattern for a real reflector by stipulating that the wide-angle radiation be less than 3 db above the ideal case. Referring to Fig. 9, one sees that for this condition to obtain, $\Delta\psi_M \approx 0.05\lambda$; therefore, since phase disturbances are roughly doubled in reflection from, say, a relatively shallow paraboloid, surface tolerance must be held to about $\pm 0.0125\lambda$.

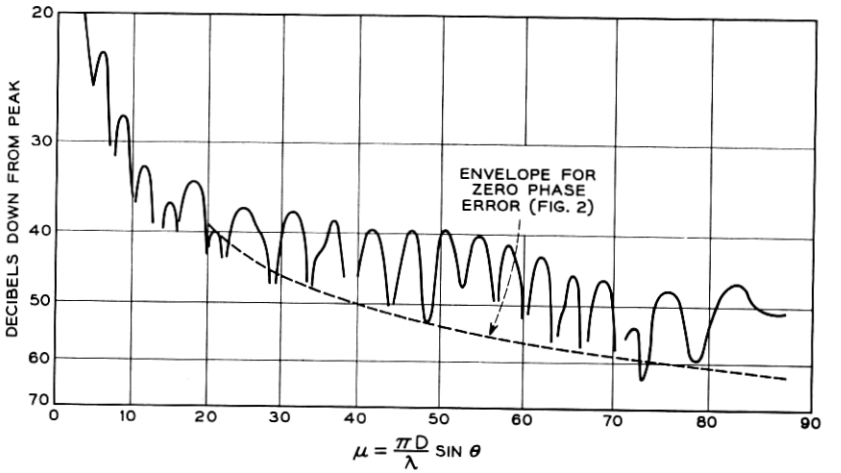

Fig. 6 — Radiation pattern: typical phase error — maximum phase error 0.155λ peak-to-peak; illumination 10-db taper.

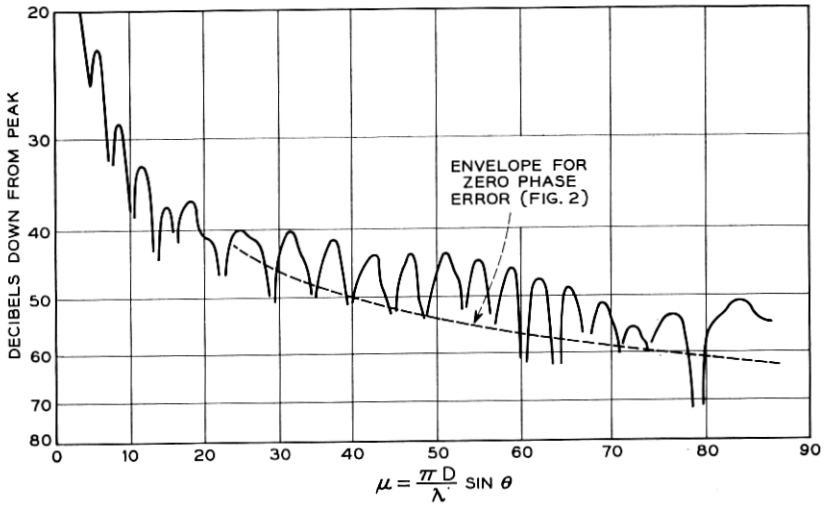

Fig. 7 — Radiation pattern: typical phase error — maximum phase error 0.1λ peak-to-peak; illumination 10-db taper.

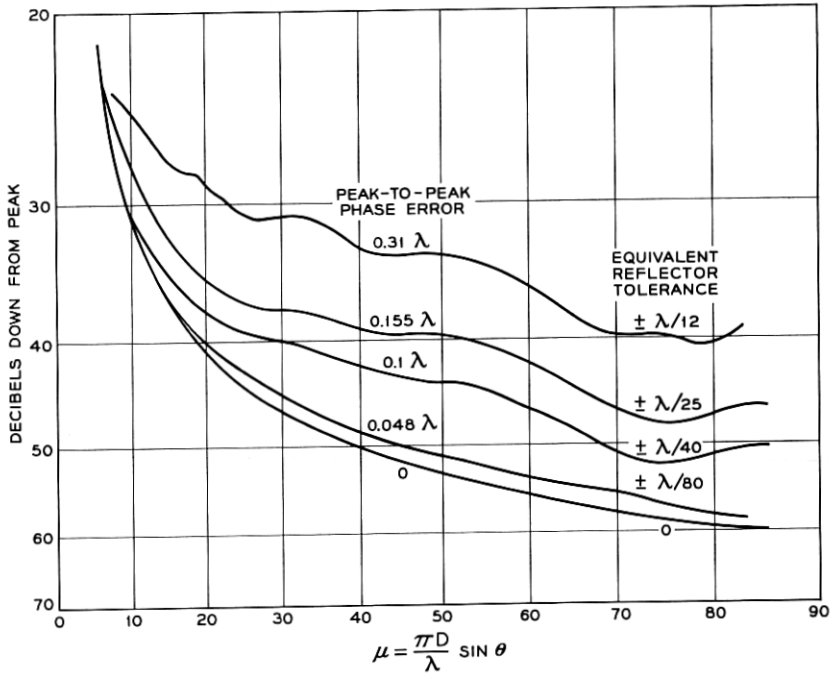

Fig. 8 — Comparison of envelopes of radiation patterns. Peak-to-peak phase errors: 0, 0.048, 0.1, 0.155, and 0.31λ; illumination 10-db taper.

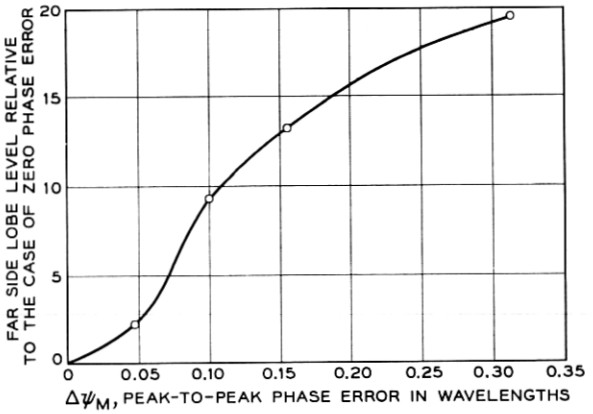

Fig. 9 — Degradation of level versus phase error for lobes at angles corresponding to

$$u = \frac{\pi D}{\lambda} \sin \theta = 50.$$

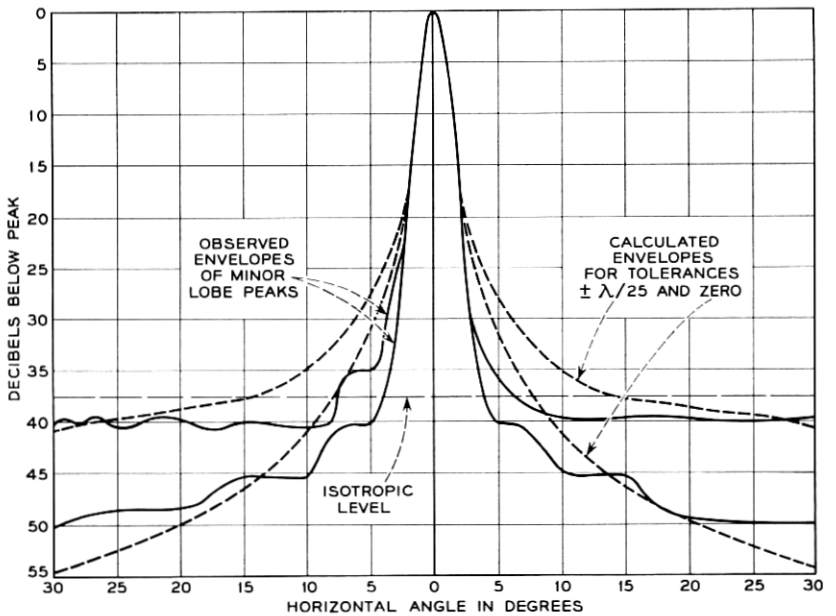

Fig. 10 — Comparison of calculated with measured patterns for precision reflector and wooden reflector with tolerance $\approx \lambda/25$.

3.3 *Comparison with Experiment*

In Fig. 10 the results of an experiment reported some years ago by H. T. Friis and W. D. Lewis[4] are shown as full curves. In that experiment the radiation patterns of two paraboloidal antennas were measured at centimeter wavelengths; one employed a searchlight mirror as a precision reflector, the other a carefully constructed metallized wooden paraboloid with the same diameter and nominal contour. The diameter of the aperture was 36 wavelengths in both cases. The data in Fig. 10 clearly show that the precision antenna has a lobe level about 10 db below that of the wooden antenna for angles $\theta = 20°$.

In Fig. 10 the measured patterns are compared with those calculated for the typical phase error of peak-to-peak value $\Delta\psi_M = 0.155\lambda$ (Fig. 6). One sees that it is possible to account for the measured increase in the side lobe level of the wooden antenna if one assumes a tolerance of about $\pm\lambda/25$ in its surface.

Of course, we realize that actual antennas, especially paraboloids, are beset with other deficiencies, such as spillover, edge currents, reradiation by feed supports, and aperture blocking, all of which give rise to wide-angle radiation. However, in the comparison experiment under discussion, these other factors are believed to be the same in the two cases.

IV. CONCLUSION

If one demands that wide-angle radiation from a reflector with quasi-random roughness be of the same order as that for a perfectly smooth surface, calculation shows that the reflector tolerance should be held to $\pm 0.01\lambda$. The calculation is verified, in part, using data obtained on paraboloidal reflectors at centimeter wavelengths. Roughness of the type described results in interference-prone microwave antennas; it also degrades their noise performance.

REFERENCES

1. Silver, S., *Microwave Antenna Theory and Design*, M.I.T. Rad. Lab. Series, 12, McGraw-Hill, New York, 1959.
2. Born, M., and Wolf, E., *Principles of Optics*, Pergamon Press, New York, 1959, p. 458.
3. Stratton, J. A., *Electromagnetic Theory*, McGraw-Hill, New York, 1941, pp. 351–364.
4. Friis, H. T., and Lewis, W. D., Radar Antennas, B.S.T.J., **26,** April, 1947, p. 265.